Line mixing in parallel and perpendicular bands of CO_2: A further test of the refined Robert-Bonamy formalism

C. Boulet,[1] Q. Ma,[2] and R. H. Tipping[3]
[1]*Institut des Sciences Moléculaires d'Orsay (ISMO), CNRS (UMR8214) and Université Paris-Sud, Bât. 350, Campus d'Orsay F-91405, France*
[2]*NASA/Goddard Institute for Space Studies and Department of Applied Physics and Applied Mathematics, Columbia University, 2880 Broadway, New York, New York 10025, USA*
[3]*Department of Physics and Astronomy, University of Alabama, Tuscaloosa, Alabama 35487-0324, USA*

(Received 3 July 2015; accepted 10 September 2015; published online 30 September 2015)

Starting from the refined Robert-Bonamy formalism [Q. Ma, C. Boulet, and R. H. Tipping, J. Chem. Phys. **139**, 034305 (2013)], we propose here an extension of line mixing studies to infrared absorptions of linear polyatomic molecules having stretching and bending modes. The present formalism does not neglect the internal degrees of freedom of the perturbing molecules, contrary to the energy corrected sudden (ECS) modelling, and enables one to calculate the whole relaxation matrix starting from the potential energy surface. Meanwhile, similar to the ECS modelling, the present formalism properly accounts for roles played by all the internal angular momenta in the coupling process, including the vibrational angular momentum. The formalism has been applied to the important case of CO_2 broadened by N_2. Applications to two kinds of vibrational bands ($\Sigma \rightarrow \Sigma$ and $\Sigma \rightarrow \Pi$) have shown that the present results are in good agreement with both experimental data and results derived from the ECS model. © *2015 AIP Publishing LLC.* [http://dx.doi.org/10.1063/1.4931587]

I. INTRODUCTION

The phenomenon of collisional transfer of intensity due to line mixing has an increasing importance for atmospheric monitoring and combustion diagnostics.[1,2] Within the limits of the impact approximation, all relevant information about the collisional processes is contained in a frequency independent relaxation matrix W, whose diagonal elements give the half-widths (and shifts) of the various lines (when they are isolated), while the off-diagonal elements correspond to line interferences.[1,3,4]

For simple systems such as those consisting of diatom-atom and diatom-diatom, accurate fully quantum calculations based on the knowledge of interaction potential surface are now feasible.[5,6] Fully quantum calculations become unfeasible for more complex systems due to large numbers of coupled channels involved. With the recent exception of the classical approach of S. Ivanov and co-workers,[7] most of the previous line mixing studies were based on semi-empirical fitting or scaling laws, such as the energy corrected sudden (ECS) model widely used in simulations of atmospheric spectra.[1,8,9] On the other hand, based on classical collisional paths and intermolecular potentials for molecular systems of interest, semi-classical approaches to calculate the relaxation matrix such as that developed by Cherkasov[10] have existed for years. The term "semi-classical" is somehow ambiguous. In this paper, "semi-classical" means that the relative motion is treated classically and the internal motion is treated quantum mechanically. Within this category, we have recently extended the Robert-Bonamy (RB) formalism to the calculation of the whole W matrix.[11,12] This formalism was first applied to the isotropic Raman spectra of self-perturbed N_2, for which a comparison with benchmark quantum results was possible.[12] The consequences of the classical path approximation were carefully analyzed. The formalism has also been extended to infrared (IR) spectra, allowing for the calculation of line coupling for P and R lines.[13] However, numerical calculations were limited to the half-widths in the particular case of $\Sigma \rightarrow \Sigma$ bands (no excited vibrational angular momentum), and it was shown that line coupling significantly reduces the half-widths when compared to the RB formulation.

In this paper, we extend the formalism to the calculation of the W matrix for vibrational bands of any symmetry ($\Sigma \rightarrow \Sigma, \Sigma \rightarrow \Pi, \Pi \rightarrow \Delta, \ldots$) and apply it to the particular case of CO_2 perturbed by N_2. As it is now well known, the analysis of the spectra of the current IR sounders have shown that line mixing is important in air-broadened CO_2 Q branches and in the wings of the bands.[2,14,15] For such a complex system, up to now, no "first principle" calculation exists. For CO_2 in a He bath, Green[16] has developed an IOS (infinite order sudden) formalism which can predict results in good agreement with data of various infrared bands and pure rotational Raman spectra. Most of this success is due to including the vibrational angular momentum into the set of coupled angular momenta. For N_2-broadening where the perturber molecular rotation plays a significant role, the IOS approximation fails because this motion has not been included in calculations. In order to remedy the problem, the ECS model was developed by introducing empirical adiabaticity factors. It should be noted that, in their first versions, the basic cross sections of the IOS and ECS formalisms were obtained from given intermolecular potentials. However, in a further step, these basic cross sections were considered as adjustable parameters. This is just the case of the ECS model of Refs. 8 and 9 and the latter has

been widely used in atmospheric simulations. Furthermore, by assimilating the latter to atoms, the ECS model neglects the internal degrees of molecular perturbers. In contrast, with the present formalism, the rotation of the molecular perturbers can be explicitly taken into account.

The present manuscript is organized in the following way. In Section II, we outline the basic of theory. The Subsection II A is devoted to a simplification treatment by Green[16] based on the fact that low lying bending modes are still nearly linear. In Section III, we describe calculations of the relaxation matrices in detail and present comparisons between calculated results for different vibrational bands of CO_2 and measured data. Subsection III G is devoted to a proposed method in order to circumvent both the limits of the semi-classical scheme and possible inaccuracies of the potential. By applying this method, we compare the present results with those obtained from the "empirical" ECS model of Refs. 8 and 9. Since that ECS model correctly predicts the experimental data, this comparison provides, in some sense, a comparison with the experimental results. Section IV consists of a brief conclusion.

II. THEORY

A. Outline of the relaxation operator W

Within the binary collisions and impact approximations, the symmetrized spectral density $\tilde{F}(\omega)$ can be written as

$$\tilde{F}(\omega) = -\frac{1}{\pi} Im \sum_{kl} \sqrt{\tilde{\rho}_l}\tilde{d}_l \left\langle l \left| \frac{1}{\omega - L_0 - i\tilde{W}} \right| k \right\rangle \sqrt{\tilde{\rho}_k}\tilde{d}_k, \quad (1)$$

where $|k\rangle$ is a vector in the line space, $\widetilde{\rho_k} = \exp\left(-\beta E_k^i\right)/Z$ is the density matrix element and E_k^i is the energy of the initial level of line k, and $\widetilde{d_k}$ is the reduced matrix element of the dipole moment (in the case of IR absorption), as adopted by Ben Reuven.[3] Note that Eq. (1) has been written in a symmetric version[12] of the formalism developed in Ref. 11. In the impact limit, a matrix element of $\tilde{W}$ may be expressed in terms of the average of the Liouville scattering operator $\hat{S}$ over the internal degrees of the bath molecule. Following Ref. 11, $\langle\tilde{S}\rangle$ is expressed via a second order cumulant expansion of the average. As shown in Refs. 11–13, the coupling and consequently line mixing result from the non-diagonality of the Liouville operator $-iS_1 - S_2$ in the line space.

Since the CO_2 molecule is allowed to bend, we need to introduce parity adapted wave functions[16] given by

$$|\nu\varepsilon j l_2 m\rangle = N_\varepsilon \left(|\nu j l_2 m\rangle + \varepsilon\,|\nu j - l_2 m\rangle\right), \quad (2)$$

where

$$|\nu j l_2 m\rangle \equiv |v_1 v_2 l_2 v_3\rangle \otimes |j l_2 m\rangle. \quad (3)$$

In the above expression, ν is a short notation for the vibrational quantum numbers v_1, v_2, and v_3, and l_2 (= $v_2, v_2 - 2, \ldots$) is the absolute value of the vibrational angular momentum. In the above expression, for $l_2 = 0$, $\varepsilon = 0$ and $N_\varepsilon = 1$ and for $l_2 \neq 0$, $\varepsilon = \pm 1$ and $N_\varepsilon = 1/\sqrt{2}$. We then follow Ben-Reuven's conventions by introducing a set of basis vectors in the line space defined by

$$\begin{aligned} |k\rangle \equiv |fi, JM_J\rangle &= |\nu_f \varepsilon_f j_f l_{2f}, \nu_i \varepsilon_i j_i l_{2i}, JM_J \gg \\ &= \sum_{m_i m_f} (-1)^{j_i - m_i} C\left(j_f j_i J, m_f - m_i M_J\right) \\ &\quad \times |\nu_f \varepsilon_f j_f l_{2f} m_f, \nu_i \varepsilon_i j_i l_{2i} m_i \gg . \end{aligned} \quad (4)$$

(In order to simplify notations, we also adopt a simple notation "i" to represent all the quantum numbers v_i, ε_i, j_i, and l_{2i}.)

Subsequently, following procedures detailed in Refs. 11–13, a matrix element of $\tilde{W}$ may be expressed in terms on the average of the Liouville scattering operator over the internal degrees of the bath molecule, expressed via a second order cumulant expansion adapted to the symmetrized version of the formalism,

$$\begin{aligned} \tilde{W}_{f'i',fi} = \frac{n_b \bar{v}}{2\pi c} \int_{r_{c,min}}^{+\infty} 2\pi (b\frac{db}{dr_c}) dr_c \\ \times \left\{ \delta_{i'i}\delta_{f'f} - \ll f'i' \left| e^{-is_1(r_c) - s_2(r_c)} \right| fi \gg \right\}, \end{aligned} \quad (5)$$

where b is the impact parameter and r_c corresponds to the point of closest approach. Note that we do not perform any thermal average over the relative kinetic energy, by restricting the calculation to its value for the mean relative velocity, $\bar{E}_{kin} = \frac{4}{\pi} k_B T$.

B. Fundamental approximations in determining potential models

In principle, for a system consisting of an absorber with excited bending modes (like CO_2) and a linear bath molecule, potential models should be written as[17]

$$\begin{aligned} V\left(\vec{R}(t)\right) = &\sum_{L_1 K_1 L_2 L} U\left(L_1 L_2 L; K_1; R(t)\right) \\ &\times \sum_{m_1 m_2 M} \mathrm{C}(\mathrm{L_1 L_2 L}, m_1 m_2 \mathrm{M}) \\ &\times \mathrm{D}^{\mathrm{L_1}*}_{\mathrm{m_1 K_1}}(\Omega_a) \mathrm{D}^{\mathrm{L_2}*}_{\mathrm{m_2 0}}(\Omega_b) \mathrm{Y}^*_{\mathrm{LM}}(\omega(t)), \end{aligned} \quad (6)$$

where $\mathrm{D}^{\mathrm{L}}_{\mathrm{mK}}(\Omega)$ are rotation matrices. However, as explained by Green,[16] since low-lying bending modes are still nearly linear, we can approximate the potential models by setting $\mathrm{K_1} = 0$ in Eq. (6). In addition, we will neglect any vibrational dependence of potential parameters. This implies that we have assumed that the potential model remains identical to that between a CO_2 molecule in a Σ state and a linear perturber and it does not have any vibrational dependences at all. In general, to neglect the vibrational dependences is not acceptable in calculating the line shift because the latter strongly depends on these vibrational dependences. But we believe these simplification assumptions would have negligible effects on calculated half-widths.[18]

Then, let us consider potential matrix elements of $\langle \nu\varepsilon' j' \mathrm{l}_2 m' | \mathrm{V} | \nu\varepsilon \mathrm{j l_2 m} \rangle$ associated with the absorber molecule. Since the potential is assumed not to act on the vibrational quantum numbers, one has

$$\begin{aligned} &\langle \nu\varepsilon' \mathrm{j' l_2} m' \,|\, \mathrm{V} |\, \nu\varepsilon j l_2 \mathrm{m} \rangle \\ &\quad = \frac{1}{2}(\langle \mathrm{j' l_2 m'} \,|\, \mathrm{V} |\, \mathrm{j l_2 m} \rangle + \varepsilon\varepsilon' \langle \mathrm{j' - l_2 m'} \,|\mathrm{V}|\, \mathrm{j - l_2 m} \rangle). \end{aligned} \quad (7)$$

Because $V \propto D^{L_1*}_{\mu_1 0}$, one can easily show that

$$\langle j' l_2 m' | V | j l_2 m \rangle = (-1)^{j+j'-L_1} \langle j' - l_2 m' | V | j - l_2 m \rangle . \quad (8)$$

With $\varepsilon = (-1)^{j+1}$ or $(-1)^j$ (depending on the type of vibrational levels) and the fact that L1 is even for a symmetric linear molecule, one obtains

$$\begin{aligned} \langle \nu \varepsilon' j' l_2 m' | V | \nu \varepsilon j l_2 m \rangle &= \frac{1}{2} \left\{ 1 + (-1)^{-L_1} \right\} \langle j' l_2 m' | V | j l_2 m \rangle \\ &= \langle j' l_2 m' | V | j l_2 m \rangle . \end{aligned} \quad (9)$$

The above relation greatly facilitates calculations of the S2 matrix elements.

We note that because the potential does not have any vibrational dependence, S_1 is zero. As for S_2, it can be written as

$$S_2 = S_{2,outer,i} + S_{2,outer,f} + S_{2,middle}. \quad (10)$$

In the present study, we will neglect imaginary parts of the matrix elements of $S_{2,\text{outer,i}}$ and $S_{2,\text{outer,f}}$. Calculations within the RB formalism have shown that these imaginary parts are of minor importance in the calculation of the half-widths,[18] and hence in that of the real part of the W matrix. As for the $S_{2,\text{middle}}$ term, both its diagonal and non-diagonal matrix elements are real.

C. Matrices of $S_{2,\text{outer,i}}$, $S_{2,\text{outer,f}}$, and $S_{2,\text{middle}}$ in the coordinate representation

In the present study, we will apply the formalism to two IR vibrational bands of CO_2, a $\Sigma \rightarrow \Sigma(l_{2i} = l_{2f} = 0)$ stretching band and a $\Sigma \rightarrow \Pi(l_{2i} = 0; l_{2f} = 1)$ bending one. Because in both cases, the initial vibrational level is the Σ fundamental one; the matrix elements of $S_{2,\text{outer,i}}$ are exactly those of a linear molecular pair and they have been already given in Ref. 13. We would like to note that because we only consider the line coupling within a given vibrational band, the matrix of $S_{2,\text{outer,i}}$ in the corresponding line space is diagonal. On the other hand, with respect to $S_{2,\text{outer,f}}$, it will depend on $l_{2f} \equiv l_2$.

One can easily show that the matrix of $S_{2,\text{outer,f}}$ is also diagonal within a vibrational band and its matrix elements are given by

$$\begin{aligned} Re S^{fi,fi}_{2,outer,f}(r_c) = \sqrt{\frac{\pi}{2}} \sum_{L_1 L_2} \sum_{i_2 i'_2} \sqrt{\tilde{\rho}_{i_2} \tilde{\rho}'_{i_2}} (2i_2 + 1)(2i'_2 + 1) \\ \times C(i_2 i'_2 L_2, 000)^2 \sum_{j'_f} (2j'_f + 1) \\ \times C(j_f j'_f L_1,\ l_2 - l_2 0)^2 \mathbb{F}_{L_1 00 L_2 0} \\ \times (\omega_{ff'} + \omega_{i_2 i'_2}) . \end{aligned} \quad (11)$$

The symmetric one dimensional (1-D) Fourier transforms $\mathbb{F}_{L_1 K_1 K'_1 L_2 K_2 K'_2}(\omega)$ are defined in the Appendix.

In contrast with the $S_{2,\text{outer,i}}$ and $S_{2,\text{outer,f}}$ terms which are diagonal within a given band, the $S_{2,\text{middle}}$ term, which is real, is always off-diagonal. It is this term that is responsible for the line coupling. The expression for its off-diagonal elements is given by

$$\begin{aligned} S^{f'i',fi}_{2,middle}(r_c) = 2\pi(-1)^{1+J}(-1)^{j_i+j'_i} \sqrt{(2j'_i+1)(2j'_f+1)(2j_i+1)(2j_f+1)} \\ \times \sum_{L_1 L_2} (-1)^{L_1} W\left(j'_i j'_f j_i j_f, J L_1\right) C\left(j_i j'_i L_1, 000\right) C\left(j_f j'_f L_1, l_2 - l_2 0\right) \\ \times \sum_{i_2 i'_2} \sqrt{\tilde{\rho}_{i_2} \tilde{\rho}'_{i_2}} (2i_2+1)(2i'_2+1) C(i_2 i'_2 L_2, 000)^2 \mathbb{F}_{L_1 00 L_2 00}\left(\frac{(\omega_{i'i} + \omega_{f'f})}{2} + \omega_{i'_2 i_2}, \omega_{fi} - \omega_{f'i'} \right) \end{aligned} \quad (12)$$

The two dimensional (2-D) Fourier transforms $\mathbb{F}_{L_1 K_1 K'_1 L_2 K_2 K'_2}(\omega, \omega')$ are also defined in the Appendix. Meanwhile, the expression for the diagonal elements of $S_{2,\text{middle}}$ becomes

$$\begin{aligned} S^{fi,fi}_{2,middle}(r_c) = (-1)^{1+J} \sqrt{2\pi} (2j_i+1)(2j_f+1) \\ \times \sum_{L_1 L_2} (-1)^{L_1} W\left(j_i j_f j_i j_f, J L_1\right) C(j_i j_i L_1, 000) C(j_f j_f L_1, l_2 - l_2 0) \\ \times \sum_{i_2 i'_2} \sqrt{\tilde{\rho}_{i_2} \tilde{\rho}'_{i_2}} (2i_2+1)(2i'_2+1) C(i_2 i'_2 L_2, 000)^2 \mathbb{F}_{L_1 00 L_2 00}\left(\omega_{i'_2 i_2}\right) . \end{aligned} \quad (13)$$

D. The sum rule and the detailed balance

In the more general fully quantum theory, *the frequency dependent* relaxation matrix has to verify some fundamental rules.[3,19–21] One is the detailed balance relationship (written here in a symmetrized form),

$$\tilde{W}_{lk}(\omega) = \tilde{W}_{kl}(\omega), \quad (14)$$

where $k \equiv \nu_f \varepsilon_f j_f l_{2f} \leftarrow \nu_i \varepsilon_i j_i l_{2i}$ and $l \equiv \nu'_f \varepsilon'_f j'_f l'_{2f} \leftarrow \nu'_i \varepsilon'_i j'_i l'_{2i}$ represent two coupled lines. Another is the sum rule representing a relationship between the diagonal element of W and a weighted sum of off-diagonal elements within the

same columns defined by

$$\tilde{W}_{kk}(\omega) = -\sum_{l\neq k} \frac{\tilde{d}_l}{\tilde{d}_k}\sqrt{\frac{\tilde{\rho}_l}{\tilde{\rho}_k}}\tilde{W}_{lk}(\omega). \quad (15)$$

However, in order to obtain tractable formalisms, people have to introduce approximations that may cause a breakdown of these fundamental rules. Among all these approximations, a very restrictive one is the impact approximation. Instead of using off-energy shell scattering amplitudes in order to account for incomplete collisions, it uses only "conventional" S matrix, consequently leading to a frequency independent W matrix. This approximation may lead to violations of the sum rule property in some cases.[20,22,23] More explicitly, it has been shown that while the sum rule remains valid in the isotropic Raman case,

$$\tilde{W}^{(0)}_{kk} = -\sum_{l\neq k}\sqrt{\frac{2j'_i+1}{2j_i+1}}\sqrt{\frac{\tilde{\rho}_l}{\tilde{\rho}_k}}\tilde{W}^{(0)}_{lk}, \quad (16)$$

it is no more valid in the IR absorption case since now,

$$\tilde{W}^{(1)}_{kk} \neq -\sum_{l\neq k}\frac{\tilde{d}_l}{\tilde{d}_k}\sqrt{\frac{\tilde{\rho}_l}{\tilde{\rho}_k}}\tilde{W}^{(1)}_{lk}. \quad (17)$$

In the above expressions, we have introduced the superscript (0) and (1) of $\tilde{W}_{lk}$ to indicate the rank of transition operators for the isotropic Raman and IR spectra, respectively.

Regarding the detailed balance principle, because we have adopted the symmetrized formalism, it becomes automatically valid since

$$\tilde{W}_{lk} = \tilde{W}_{kl}. \quad (18)$$

Although initial correlations have been neglected, as well as the average over the kinetic energy, one may expect that inaccuracies caused by these neglects will be partially compensated by adopting the symmetrized form of the theory.

There is another difficulty to be wary of that results from the semi-classical approximation. As shown in our previous work on the isotropic Raman spectra of N_2,[12] the calculated W matrix does not exactly verify Eq. (16) since one has only

$$\tilde{W}^{(0)}_{kk} = -\sum_{l\neq k}\sqrt{\frac{2j'_i+1}{2j_i+1}}\tilde{W}^{(0)}_{lk}. \quad (19)$$

Indeed, the present classical path formalism assumes that the molecules can make inelastic transitions without any effect on their translational energy. This approximation, very common in semi classical theories, is justified if the inelastic transitions involve energy changes which are small compared with k_BT. Then, small changes in translational energy cause small changes in the trajectory. One will obtain Eq. (19) from Eq. (16) by assuming that $|E^i_l - E^i_k| \ll k_BT$, so that $\tilde{\rho}_l/\tilde{\rho}_k \approx 1$.[24] In some sense, Eq. (19) can be called as the semi-classical approximation of Eq. (16).

These intrinsic weaknesses may limit the reliability of the semi-classical formalism. Methods correcting for effects of inelasticity were analyzed in Ref. 12. Another procedure to force the IR W matrix to verify exactly Eq. (15) will be presented in Sec. III G.

III. CALCULATIONS OF THE RELAXATION MATRIX

A. The coupling strength factor

Before carrying out complicated calculations involving collisional dynamics, it is worthwhile to do a simple and helpful evaluation first. As shown in Eq. (12), contributions to the off-diagonal elements between two coupled lines from a specified correlation function of order L_1 are proportional to a factor $\sqrt{(2j'_i+1)(2j'_f+1)(2j_i+1)(2j_f+1)}W\left(j'_ij'_fj_ij_f, JL_1\right)$ $C\left(j_ij'_iL_1,000\right)C\left(j_fj'_fL_1,l_2-l_20\right)$. We call it as the coupling strength factor between the two lines of $j'_f \leftarrow j'_i$ and $j_f \leftarrow j_i$. As shown in its definition, it contains information of the angular momentum couplings between all angular momenta of the absorber molecule. In cases of this factor is zero or negligible, one can ignore the line coupling between them. As shown in its definition, it is easy to calculate the coupling strength factor because the calculation does not involve any dynamics. However, the results would be very helpful to determine in advance that among all possible coupled pairs, which of pairs are required to be considered and which can be simply ignored.

As example, in Fig. 1, we present values of the strength factor with $L_1 = 2$ for the R − R and R − P couplings in $\Sigma \rightarrow \Sigma$ bands. For the R − R coupling, because values of the strength factor are negative, we plot their absolute values between R(J) and R(J + 2) lines with J = 0, 2, ... As shown in the figure, the values vary within a narrow region and after J ≥ 8, they reach at an asymptotic constant (−1.8750). On the other hand, there is a completely different story for the R − P coupling. In this case, there are two sets of calculated values consisting of results between R(J) and P(J + 2) lines with J = 0, 2, . . . and that between R(J) and P(J) lines with J = 2, 4, ... As shown in the plot, starting from their maximum values (i.e., 1.4142 and 0.3499) reached at their lowest J = 0 and J = 2, respectively, these values decrease very quickly and both of them become less than 0.01 when J ≥ 14, due to the $W\left(j'_ij'_fj_ij_f, JL_1\right)$ coefficient. This implies that significant R − P coupling could only occur between those lines with J < 14. It is known[1,8,9,16] that in comparison with the R − R and P − P coupling, the R − P coupling is much weaker. Based on these discussions,

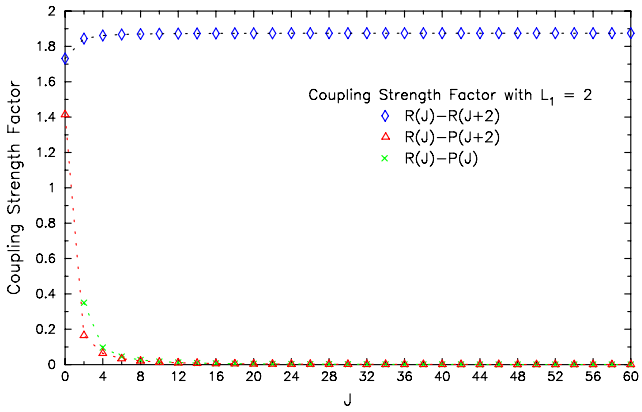

FIG. 1. The coupling strength factors with $L_1 = 2$ for R(J) − R(J + 2), R(J) − P(J + 2), and R(J) − P(J) couplings in $\Sigma \rightarrow \Sigma$ bands. They are plotted by ◇, Δ, and ×, respectively.

one concludes that it is the strength factor, or more precisely, it is the angular momentum couplings of the absorber molecule that plays a crucial damping role in decoupling R and P lines.

B. The potential and trajectory models

Next, before presenting dynamic calculations, we briefly outline the potential and the trajectory models used in these calculations. For the CO_2 and N_2 pair, people usually adopt potential models consisting of the isotropic and anisotropic parts. The isotropic part plays a decisive role in determining collisional trajectories and usually takes a standard LJ (12-6) form with two parameters σ_{traj} and ε_{traj}. Meanwhile, the anisotropic part consists of a long-range leading quadrupole-quadrupole interaction and a short-range atom-atom model given by

$$\begin{aligned} V_{atom-atom} &= \sum_{i\in a}\sum_{j\in b} 4\varepsilon_{ij}\left\{\frac{\sigma_{ij}^{12}}{r_{ij}^{12}} - \frac{\sigma_{ij}^{6}}{r_{ij}^{6}}\right\} \\ &= \sum_{L_1K_1L_2L}\sum_{n_{(ij)}}\sum_{wq}\frac{\mathcal{U}\left(L_1K_1L_2L, n_{(ij)}, wq\right)}{R(t)^{L_1+L_2+q+2w}} \\ &\quad\times \sum_{m_1m_2m} C\left(L_1L_2L, m_1m_2m\right) \\ &\quad\times \mathrm{D}^{\mathrm{L_1}*}_{\mathrm{m_1K_1}}(\Omega_a)\,\mathrm{D}^{\mathrm{L_2}*}_{\mathrm{m_20}}(\Omega_b)\,\mathrm{Y}^{*}_{\mathrm{Lm}}(\omega(t)), \end{aligned} \tag{20}$$

where ε_{ij} and σ_{ij} are parameters and r_{ij} are distances between the i-th atom of the absorber molecule a and the j-th atom of the bath molecule b. In the second line of Eq. (20), the atom-atom model is given in terms of the spherical expansions where $n_{(ij)}$ runs over all pairs of i and j, q = 6 or 12, w is the integer index from 0 to infinity, and the definition of $\mathcal{U}\left(L_1K_1L_2L, n_{(ij)}, wq\right)$ can be found in the literature.[25,26] Since we do not intended to optimize potentials in the present study, we select potential parameters available in the literature. In the present study, we have used a potential model determined by Bouanich[27] by fitting experimental data of the second virial coefficients. The isotropic part determines collisional trajectories and takes a standard LJ(12-6) form with two parameters σ_{traj} and ε_{traj}, determined by fitting the isotropic part of the atom-atom potential with a LJ(12-6) form. Table I gives the potential parameters for the CO_2–N_2 pair. According to our assumption on the potential, these parameters are independent on the vibrational quantum numbers.

We have chosen 4 as the cutoff for the tensor ranks of L_1 and L_2 in the spherical expansion of the atom-atom model. Thus, there are six correlations and six Fourier transforms considered in the calculations and they are labeled by (22) (i.e., $L_1 = 2$, $L_2 = 2$), (20), (40), (42), (24), and (44), respectively. With respect to another cutoff for setting the upper limit for w, in contrast with the standard RB formalism, selecting a higher cutoff does not add more computational burdens because the coordinate representation has been introduced in developing the formalism.[11–13] In the present study, we have used the 20-th cutoff (i.e., to set 20 as the maximum of 2w). The convergence of these cutoffs has been checked.

Finally, concerning the trajectory, we have adopted an "exact" model. Of course, as outlined above, the trajectory model is not really "exact" because in evaluating trajectories, effects from anisotropic interactions have been completely ignored since trajectories are driven only by the isotropic part of the potential. Meanwhile, in order to technically cover all important trajectories well, we have selected 600 values for r_c with more dense points to depict nearly head-on collisions than glancing collisions.

C. The calculated 2-D Fourier transforms

In the present study, main computation tasks are derivations of the correlation functions and their Fourier transforms. After the 2-D Fourier transforms of $F_{L_100L_200}(\omega,\omega')$ are available, one can calculate the off-diagonal elements of S_2 with Eq. (12). As shown in Eq. (12), besides of the strength factor, contributions to the off-diagonal elements of S_2 from the potential components with specified tensor ranks of L_1 and L_2 are determined by values of $\mathbb{F}_{L_100L_200}\left((\omega_{i'i} + \omega_{f'f})/2 + \omega_{i'_2i_2}, \omega_{fi} - \omega_{f'i'}\right)$. In order to quantitatively understand the role played by them, it is necessary to provide profiles of these Fourier transforms together with how the average energy gap defined by $(\omega_{i'i} + \omega_{f'f})/2$ and the frequency gap defined by $\omega_{fi} - \omega_{f'i'}$ would vary as the pair of interest varies. As clearly shown in the above expressions, the averaged energy gap is a main part of the first argument of $F_{L_100L_200}$ and the frequency gap is their second argument.

Based on the potential model, one can find the minimum of the closest distance for the "exact" trajectories at T = 296 K is $r_{c,\min}$ = 3.831 Å. Because nearly head-on collisions play a dominant role in the line coupling, we select a trajectory with r_c = 4.0 Å as example. Then, among all the Fourier transforms, we consider the dominant one with $L_1 = 2$ and $L_2 = 0$ and in Fig. 2, we present its three dimensional plot $\mathbb{F}_{200000}(k,k')$ with the dimensionless arguments $k = (r_c\omega/\bar{v})$ and $k' = (r_c\omega'/\bar{v})$ which are commonly used in numerical calculations. This plot provides a complete picture about how its magnitudes vary with the two variables k and k' at this specified trajectory. As shown in Fig. 2, roughly speaking after $|k| > 12.5$ or $|k'| > 22.5$, magnitudes of $\mathbb{F}_{200000}(k,k')$ would decrease to 10% of its perk value. This implies that the magnitudes could still remain significant as long as $|k| < 12.5$ and $|k'| < 22.5$. For the specified conditions of the plot (i.e., r_c = 4.0 Å and T = 296 K), the value convert

TABLE I. Potential parameters of the CO_2–N_2 pair.

$\Theta(CO_2)$ (esu)	$\Theta(N_2)$ (esu)[a]	ε_{CN}/k_B (K)	σ_{CN} (Å)	ε_{ON}/k_B (K)	σ_{ON} (Å)	ε_{traj}/k_B (K)	σ_{traj} (Å)
-4.02×10^{-26}	-1.35×10^{-26}	51.28	3.42	43.9	3.148	134.325	4.027

[a]Value of $\Theta(N_2)$ comes from Ref. 28 and that of $\Theta(CO_2)$ from Ref. 18.

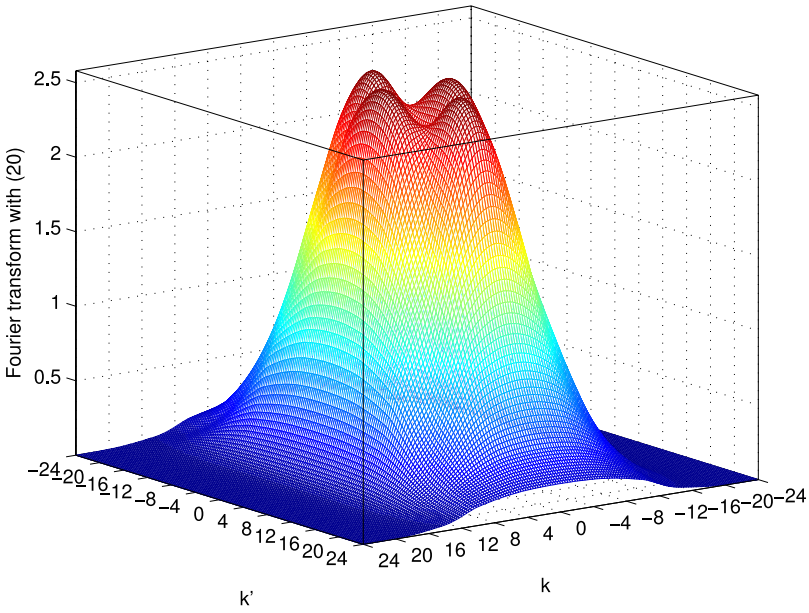

FIG. 2. The 2-D Fourier transform $\mathbb{F}_{200000}(k,k')$ (in ps^{-2}) at T = 296 K for a molecular pair of CO_2–N_2. The calculation is based on the "exact" trajectory model with $r_c = 4.0$ Å.

from ω (in cm^{-1}) to k (dimensionless) is $k \approx 0.124 \times \omega$. Then, we obtain two characteristic parameters of 100 cm^{-1} and 180 cm^{-1} as numerical measures such that, as long as the first and second arguments of $F_{200000}(\omega,\omega')$ in Eq. (12) are individually less than their measures, one must consider the off-diagonal elements of S_2. The latter implies that the line coupling does occur. It is worth mentioning that in the present study, the most part of discussions, including the derivations of these two parameters, are carried out in the frequency domain. But, it would be helpful to explain their dynamical nature in the time domain. In fact, they represent how an overlap between the same specified component of $V(\vec{R}(t))$ and $V(\vec{R}(t'))$ varies along a specified collision trajectory.

For the CO_2 molecule, the rotational constant B is around 0.4 cm^{-1}. Let's consider the R − R coupling in $\Sigma \rightarrow \Sigma$ band first. For the R(J) − R(J + 2) coupling, the averaged energy gaps are ±4(J + 2)B and the frequency gaps are constant ±4B (i.e., ±1.6 cm^{-1}). At $r_c = 4.0$ Å, 1.6 cm^{-1} corresponds to $k' = 0.2$. Then, one can conclude that for the R − R coupling, the coupling importance is solely determined by values of the averaged gap and the latter is judged by the threshold around 100 cm^{-1}. Based on these numbers, one expects that at least up to J = 64, the off-diagonal elements of S_2 between two R lines remain significant.

For the R − P coupling, as explained above, mainly due to the damping effect from the strength factor, the coupling between lines with J > 14 becomes negligible. In this case, we only need to focus attention to lower J lines. For R(J) − P(J + 2) coupling, the averaged energy gap and the frequency gap are ±(2J + 3)B and ±2(2J + 3)B, respectively. For coupled lines with J < 14, values of these two gaps are much less than their thresholds 100 cm^{-1} and 180 cm^{-1}. This implies that the 2-D Fourier transforms would not add a new restriction to the R − P coupling for such J values. Based on these discussions, we can conclude that the off-diagonal elements of S_2 between R and P lines with J < 14 remain significant.

Finally, because the rotational constant of CO_2 is very small, many rotational states are significantly populated (up to J ≅ 120 at room temperature). By considering this fact together with those discussed above, one can draw two conclusions. First of all, one must consider the line coupling for CO_2 lines. Second, the sizes of line spaces spanned by coupled CO_2 lines would be pretty large.

The procedure to evaluate of the matrix elements of $S_{2,\text{outer,i}}$ and $S_{2,\text{outer,f}}$ is the same as that reported in our previous works.[11–13] Because the matrix of $-S_2$ is a real and symmetric matrix, one can easily obtain the matrix elements of $\exp(-S_2)$ by carrying out a unitary transform. Alternatively, there is a subroutine F10ECF available in NAG which enables one to directly calculate them.

In the present study, for the $\Sigma \rightarrow \Sigma$ band, we have considered a (122 × 122) W matrix in a lines space constructed by R(0), P(2), R(2), . . . , R(120), and P(122) lines. Meanwhile, for the $\Sigma \rightarrow \Pi$ band, the (183 × 183) W matrix was constructed by R(0), P(2), Q(2), . . . , R(120), P(122), and Q(122). In addition, for isotropic Raman band, we have taken into account of Q(0), Q(2), . . . , Q(118), and Q(120) lines and the size of

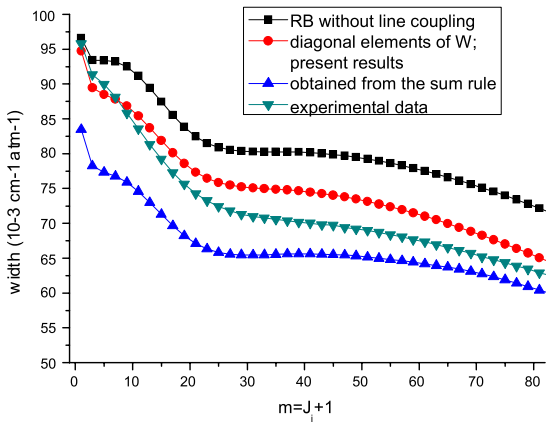

FIG. 3. Influence of line coupling on the calculated half-widths for the R-branch in $\Sigma \rightarrow \Sigma$ band. The experimental data are from Ref. 35.

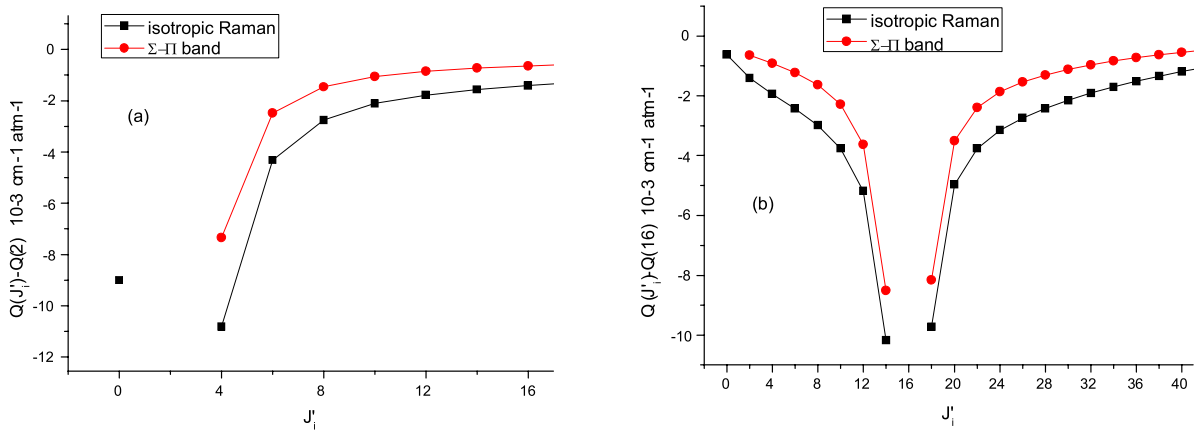

FIG. 4. Relaxation matrix elements of the Q(2) and Q(16) lines coupled to other Q(J′) transitions. They are presented in Figs. 4(a) and 4(b), respectively.

the calculated W matrix is 61×61. All of these calculated W matrices will be provided in the supplementary material.[37]

D. Calculated diagonal elements of the relaxation matrix W

Fig. 3 illustrates the influence of the line coupling (i.e., of the non-diagonality of S_2 within the line space) on calculated half-widths for the R-branch in $\Sigma \rightarrow \Sigma$ band. As expected from previous works,[12,13] calculated values are significantly reduced by around 8% and become closer to measurements. Effects of similar amplitude were obtained for other bands with different symmetries. This corroborates once more the importance of taking into account the non-diagonality of S_2 in the half-width calculation, illustrating one of the weaknesses of the RB formalism.

With respect to the sum rule, while the semi-classical sum rule (Eq. (19)) is exactly verified in the isotropic Raman case, as previously observed for N_2,[12] in the case of IR absorption, and within the semi-classical approximation, one can see that

$$\tilde{W}^{(1)}_{kk} \neq -\sum_{l \neq k} \frac{\tilde{d}_l}{\tilde{d}_k} \tilde{W}^{(1)}_{lk}. \tag{21}$$

As has been noted previously,[8,19,20,23] such defect could lead to important artifacts in the calculation of the near wings of vibrational bands.

E. Calculated off-diagonal elements of the relaxation matrix W

The off-diagonal elements coupling Q(2) and Q(16) lines to the other Q(J′) lines in a $\Sigma \rightarrow \Pi$ band are compared with similar elements for isotropic Raman diffusion ($l_{2i} = l_{2f} = 0$) in Figs. 4(a) and 4(b), respectively. These figures demonstrate the very significant dependence on the type of spectroscopy (i.e., rank of the tensor coupling matter to radiation) through the vibrational angular momentum involved in the transitions.

In Fig. 5, we present off-diagonal elements between R(4) and other R(J′) lines (i.e., the intra-branch coupling) obtained for two bands with different symmetries. In Fig. 6, we present similar results between R(4) and P(J′) lines (i.e., inter-branch coupling). As shown in the figures, while the l_2-dependence is weak in the intra-branch coupling, it becomes strong in the inter-branch coupling.

Now, we consider the coupling of R(16) to the other R(J′) lines and the coupling of R(16) to P(J′) lines. These results are presented in Figs. 7 and 8, respectively, and in general, they are similar to those in Figs. 5 and 6. Note that the inter-branch coupling at high J values is negligible that is consistent with the conclusion previously draw from the analysis of the strength factor. On the opposite (cf. Figs. 5 and 6), the difference between the inter- and the intra-branch couplings is smaller at low J values. The differences between

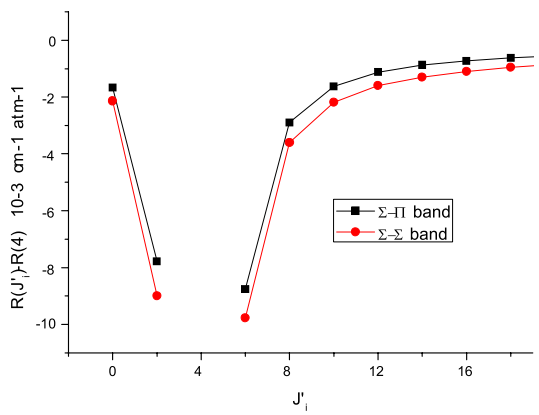

FIG. 5. Intra-branch coupling; relaxation matrix elements between R(4) and other R(J′) transitions.

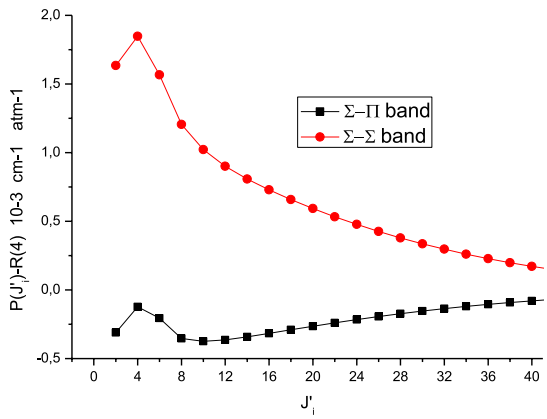

FIG. 6. Inter-branch coupling; relaxation matrix elements between R(4) and P(J′) lines.

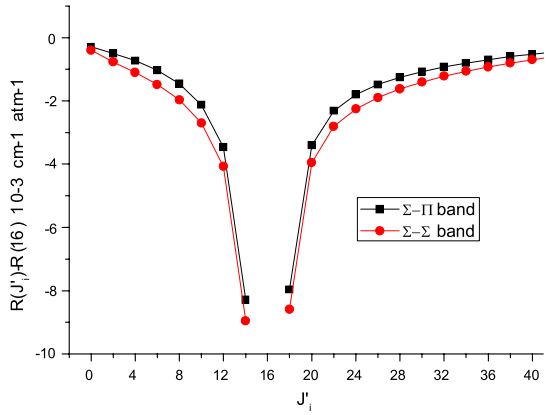

FIG. 7. Intra-branch coupling; relaxation matrix elements between R(16) and other R(J′) lines.

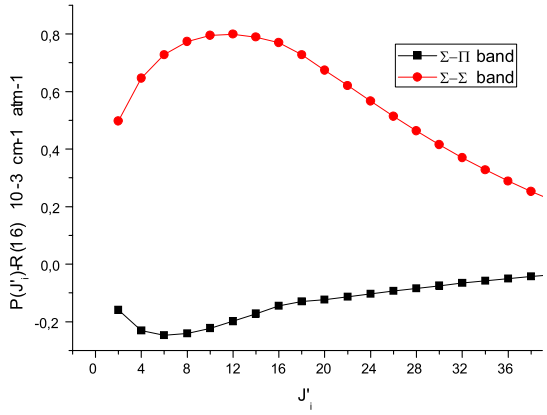

FIG. 8. Inter-branch coupling; relaxation matrix elements between R(16) and P(J′) lines.

inter- and intra-branch couplings at low and high J values are also demonstrated in Figs. 9 and 10 in which the couplings of Q(2) and Q(16) to all other lines in Σ → Π band are presented. All of these properties have also been observed both within the ECS approach,[29] a semi-classical model,[30] or a fully quantum calculation[31] (for simpler systems). By properly taking into account of the coupling of various angular momenta involved, the present model enables one to predict intra-branch as well as inter-branch coupling elements. It is worth mentioning that the full collapse of the various branches into a single feature at very high perturber densities is a direct consequence of inter-branch coupling.[32,33]

F. The sum rule

Finally, we present a comparison between calculated diagonal elements and the results of the sum rules (Eq. (20)) for two different vibrational bands in Fig. 11. Although off-diagonal elements depend on the vibrational angular momentum, both the diagonal ones and the sum rules only slightly depend on l_2. As already discussed, the difference between the diagonal elements and the results derived from the sum rule is a consequence of the impact approximation.

G. Comparison with ECS formalism

As outlined in the Introduction, the necessity of considering the line mixing in the atmospheric IR spectra of CO_2 has been firmly established. But, due to the complexity of the CO_2-air system, only approximate methods are available right now. Among them, the ECS model is one of the most successful approaches. Therefore, it would be helpful to compare the present results with those obtained with the adjusted ECS model of Refs. 8 and 9. We recall here the main features of the ECS model. First of all, it must be pointed out that the ECS formalism is developed within the Gordon's convention[4,12] based on an unsymmetrized formalism where the spectral density F(ω) is given by

$$F(\omega) = -\frac{1}{\pi} Im \sum_{kl} \rho_k d_k d_l \langle l \left| \frac{1}{\omega - L_0 - iW} \right| k \rangle, \quad (22)$$

where $\rho_k = (2j_i + 1)\tilde{\rho}_k$ is the population of the initial level of line k and $d_k = \tilde{d}_k / \sqrt{(2j_i + 1)}$ is the reduced dipole moment as defined by Shafer and Gordon.[4] Within the approximations detailed in Ref. 8, the coupling between two allowed infrared transitions of a given vibrational band with any symmetry is given by

$$W_{l,k} = (-1)^{l_i + l_f} \left(2j_i' + 1\right) \sqrt{\left(2j_f + 1\right)\left(2j_f' + 1\right)} \times \sum_{L\ even \neq 0} \begin{pmatrix} j_i & L & j_i' \\ l_i & 0 & -l_i \end{pmatrix} \begin{pmatrix} j_f & L & j_f' \\ -l_f & 0 & l_f \end{pmatrix} \begin{Bmatrix} j_i & j_f & 1 \\ j_f' & j_i' & L \end{Bmatrix} (2L + 1)\, Q\,(L)\, \frac{\Omega\,(j_i, d_c)}{\Omega\,(L, d_c)}, \quad (23)$$

where ( ) and { } are 3J and 6J coefficients, respectively, $l_i \equiv l_{2i}$, and $l_f \equiv l_{2f}$. The adiabaticity factor Ω is written in terms of a scaling length d_c. They are defined in Ref. 8 together with the basic rates Q(L) which are expressed through an exponential-power law. In addition, let's emphasize that this equation is used for downward transitions (defined by $j_i' < j_i$) only, and the upward ones are obtained from detailed balance,

$$W_{lk}\rho_k = W_{kl}\rho_l. \quad (24)$$

The parameters of the exponential-power law together with the scaling length have been determined from fitting experimental half-widths by using the sum rule,

$$W_{kk} = -\sum_{l \neq k} \frac{d_l}{d_k} W_{lk}. \quad (25)$$

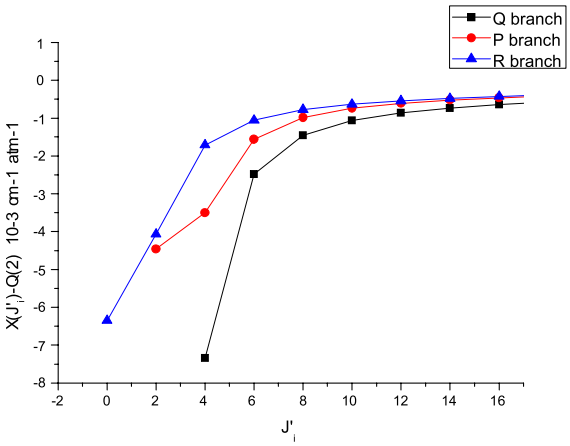

FIG. 9. Relaxation matrix elements between Q(2) and all the other lines in $\Sigma \rightarrow \Pi$ band.

The optimized parameters, which are given in Refs. 8 and 9, can reproduce the input broadening data with an accuracy around 10%. However, as already mentioned, the calculation of the wings is extremely sensitive to the accuracy of the sum rule which must be verified with an accuracy higher than 1%. The choice made in Ref. 8 was then to force the non-diagonal elements to reproduce *exactly* the experimental half-widths through a renormalization procedure detailed in that reference. (Note that an alternative solution exists: replacing the input broadening data by the results of the fit. But in that case, isolated lines will be less correctly modeled since their half-widths may differ from the experimental values by about 10%.)

Some difficulties exist when one wants to compare the adjusted-ECS and present predictions.

(1) As it appears by comparing Eqs. (1) and (22), the spectral density is not written within the same convention. Assuming the equivalence of the two spectral densities, Appendix A of Ref. 12 recalls how to retrieve the relation between $\tilde{W}_{lk}$ (present theory) and W_{lk} (ECS),

$$W_{lk} = \sqrt{\frac{\rho_l}{\rho_k}}\tilde{W}_{lk}. \tag{26}$$

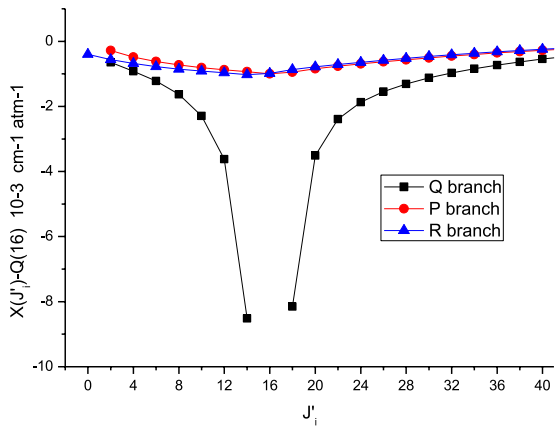

FIG. 10. Relaxation matrix elements between Q(16) and all the other lines in $\Sigma \rightarrow \Pi$ band.

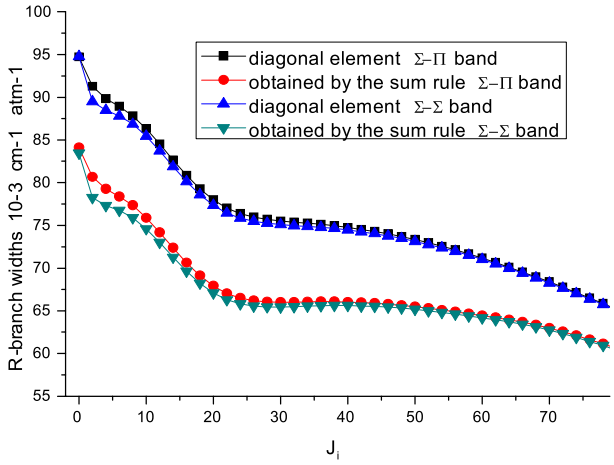

FIG. 11. Comparison between the diagonal elements of the relaxation matrix with the results of the sum rule (Eq. (19)) for the R branches of two vibrational bands of CO_2.

(2) As shown above, in the impact limit, the sum rule is not exactly verified, while in the ECS model, it is automatically verified since the diagonal elements are deduced from the sum rule (Eq. (25)).

(3) Finally, even if the intermolecular potential we used here gives a reasonable description of the virial coefficients, its accuracy remains questionable as well as that of the present theory itself.

To overcome these difficulties and perform a significant comparison, by starting from the $\tilde{W}_{lk}$ matrix elements, we have used the following procedure.

(1) We assume that downward elements ($j_i' < j_i$) may be obtained from the semi-classical approximation of Eq. (26), namely,

$$W_{lk} = \sqrt{\frac{2j_i' + 1}{2j_i + 1}}\tilde{W}_{lk}. \tag{27}$$

(2) Then, upward elements W_{lk} were built from detailed balance (Eq. (24)).

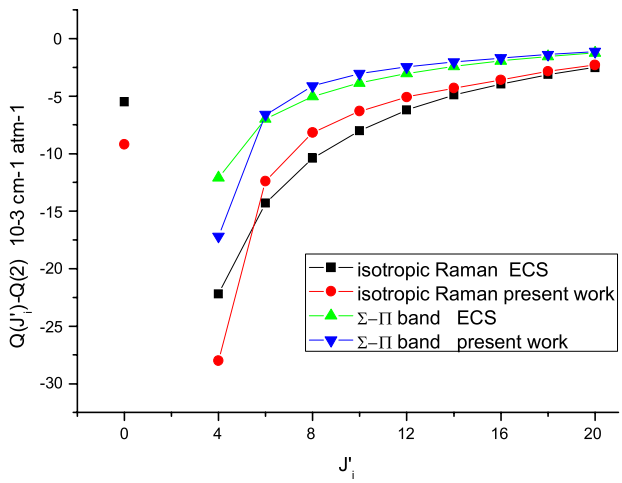

FIG. 12. Comparison between ECS and present results. Relaxation matrix elements coupling Q(2) to the other Q(J′) lines.

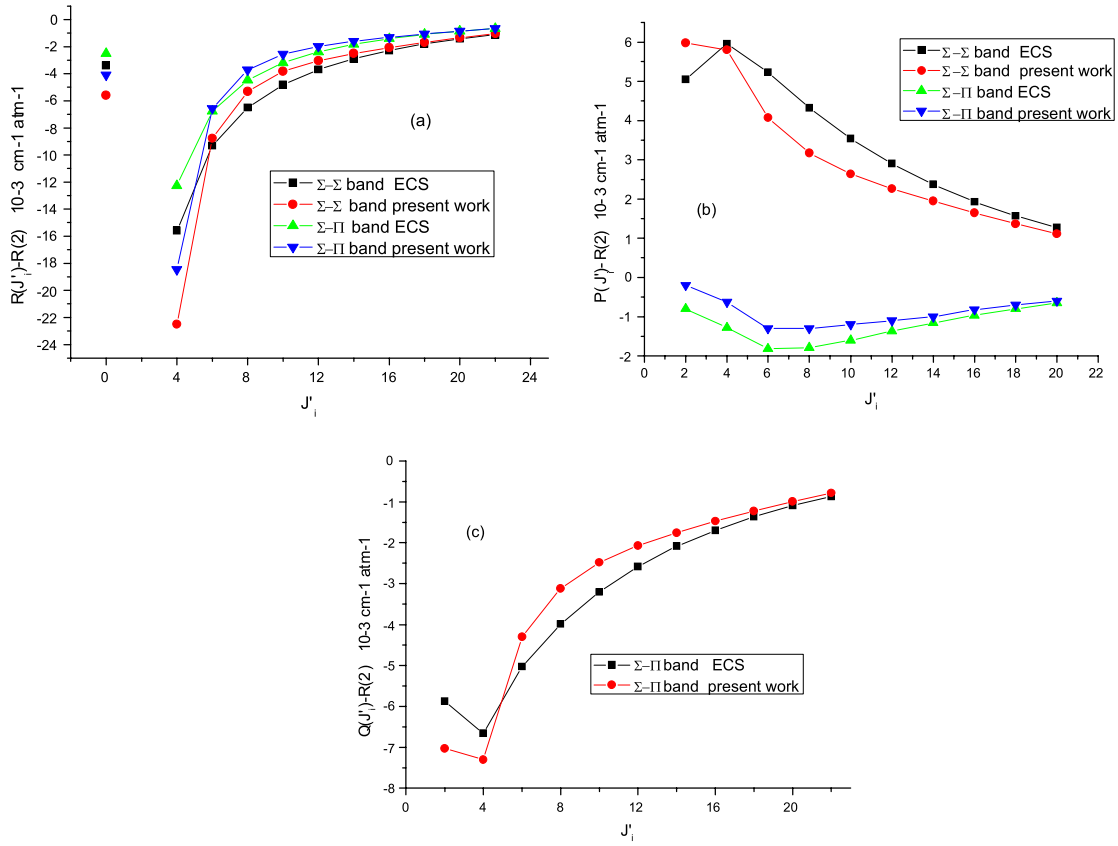

FIG. 13. Comparison between ECS and present results. Relaxation matrix elements coupling R(2) (a) to the other R(J′) lines; (b) to P(J′) lines; (c) to Q(J′) lines in $\Sigma \rightarrow \Pi$ band.

(3) Then, a renormalization procedure similar to that introduced by Niro *et al.* in their ECS approach[8] was used, forcing the off-diagonal elements to reproduce exactly the observed half-widths via the sum rule (Eq. (25)).

A meaningful comparison with the ECS model then becomes possible since the two formalisms respect the detailed balance, verify exactly the sum rule, and provide exactly the same half-widths. Some comparisons are given in Figs. 12–15. Fig. 12 shows a comparison between ECS and present off-diagonal elements between Q(2) and Q(J′) lines for isotropic Raman diffusion and in $\Sigma \rightarrow \Pi$ band. Both the rotational and l_2 dependences are quite identical even if differences between the two formalisms may punctually exist together with compensating effects at the level of the sum rule (since the half-widths resulting from the sum rule are identical).

We now consider the coupling of R(2) to the other branches in the two cases of $\Sigma \rightarrow \Sigma$ and $\Sigma \rightarrow \Pi$ bands. The conclusions already obtained from the analysis of Fig. 12 are similar for Fig. 13(a). Figure 13(b) shows that the strong l_2 dependence of the R – P coupling is quite identical in the two approaches, and the same is true for R – Q coupling as it appears in Fig. 13(c). Fig. 14 shows a similar agreement for the coupling of R(16) to the other R(J′) illustrating the case of high J values.

It should be noted that the l_2 dependence is handled very differently in the two approaches. In an ECS off-diagonal W element (Eq. (23)), the coupling between the angular momenta appears in each L component via the product,

$$\begin{pmatrix} j_i & L & j_i' \\ l_i & 0 & -l_i \end{pmatrix} \begin{pmatrix} j_f & L & j_f' \\ -l_f & 0 & l_f \end{pmatrix} \begin{Bmatrix} j_i & j_f & 1 \\ j_f' & j_i' & L \end{Bmatrix}, \tag{28}$$

where L is the order of the corresponding basic rates. In the present theory, the coupling appears at an earlier step, via the strength factor in the expression of the non-diagonal element of $S_{2,\text{middle}}$ (Eq. (12)) with a similar product of 3j and 6J symbols but with L replaced by L_1 which is the rank of the component of the intermolecular potential. Then, the exponentialization

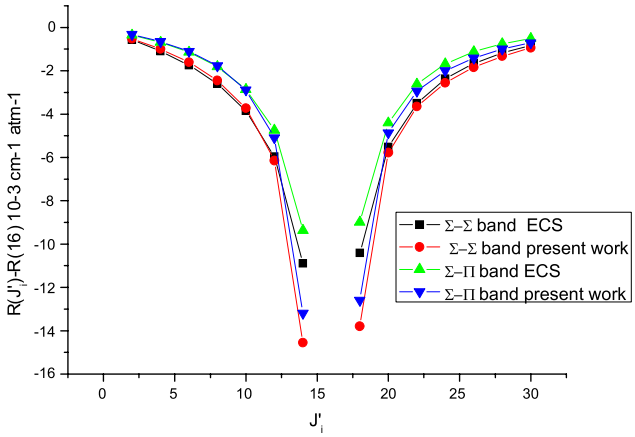

FIG. 14. Comparison between ECS and present results. Relaxation matrix elements coupling R(16) to the other R(J′) lines.

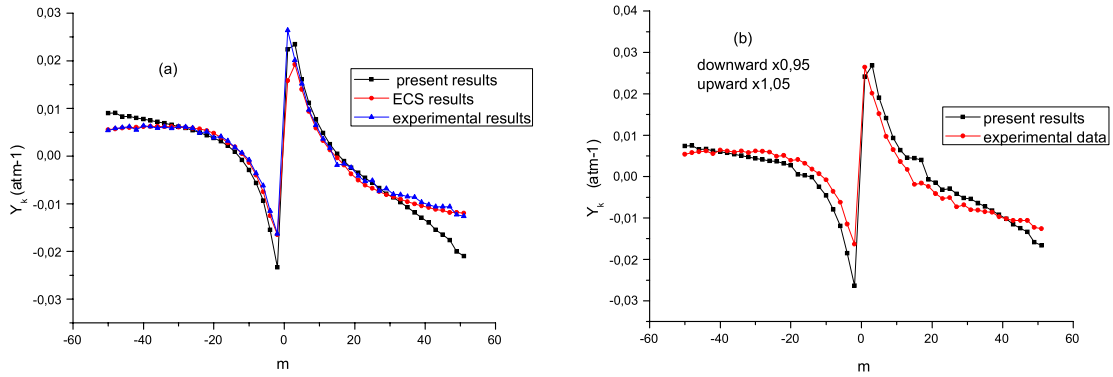

FIG. 15. Comparison of first order line mixing coefficients from ECS model and present theory with experimental values from Ref. 34 ($m = -J_i$ for P lines and $m = J_i + 1$ for R lines) in $\Sigma \rightarrow \Sigma$ band. (a) Initial calculation; (b) downward elements reduced by 5% and upward elements increased by 5%.

of $-S_2$ is believed to lead to the good agreement observed between the two approaches.

Finally, as shown in Fig. 15(a), there is also a reasonable agreement between the theoretical first-order line mixing coefficients Y_k predicted by the ECS and present models and defined by

$$Y_k = 2 \sum_{l \neq k} \frac{d_l}{d_k} \times \frac{W_{lk}}{\omega_k - \omega_l} \tag{29}$$

and also with those recently measured from multispectrum analyses of laboratory spectra in $\Sigma \rightarrow \Sigma$ bands.[34] Of course, some discrepancies appear at high J values which indicate that the amplitudes of the downward cross sections are a little bit too high and/or the amplitudes of the upward ones are a little bit too small. This may be related to the crudeness of the procedure used here in proceeding from the symmetrized to the unsymmetrized form of the formalism, as well as to approximations remaining in the present formalism, which include neglect of the average over the relative kinetic energy, uncertainties in the intermolecular potential, neglect of energy exchange between translation and rotation. The great sensitivity of the Rozenkranz parameters Y_k at high J values must be emphasized since it appears from Fig. 15(b) that a very small variation (5%) of the non-diagonal elements leads to mixing coefficients in much better agreement with the experiment. On the basis of the very reasonable agreement observed between the W matrices calculated by the present and the adjusted-ECS models, one can ascertain that no significant difference would occur in the next step: the calculation of synthetic CO_2 spectra.

IV. CONCLUSION

We have presented an extension of the semi-classical calculations of the relaxation matrix of Refs. 11 and 12 to all types of IR bands. The parallel ($\Sigma \rightarrow \Sigma$) and the perpendicular ($\Sigma \rightarrow \Pi$) bands of CO_2 have been successfully studied and results are compared with previous ECS calculations and experimental data. It has been shown that, as the ECS approach, the present formalism properly includes the vibrational angular momentum into the scheme of coupling of angular momenta. The present formalism can be applied to other IR vibrational bands ($\Pi \rightarrow \Pi, \Pi \rightarrow \Delta, \ldots$) as well as to anisotropic Raman spectra. Moreover, because the formalism can consider the internal degree of molecular perturbers, it can be applied, for example, to the case of CO_2 perturbed by H_2O, which may have some influence in humid atmospheres.[2] Another topic of interest in future studies is calculations of the imaginary part of the relaxation matrix from known potential energy surfaces. At present, some approaches to pursue this question are in progress, such as a generalized ECS formalism.[36] However, to the best of our knowledge, no calculations of the complex W matrix exist for complicated molecular systems starting from the intermolecular potential. Of course, the present formalism remains a semi-classical approach, and consequently, it would be very worthwhile to find solutions to force the formalism to verify fundamentals rules.

ACKNOWLEDGMENTS

Two of the authors (Q. Ma and R. H. Tipping) acknowledge financial support from NSF under Grant No. 1228861. This research used resources of the National Energy Research Scientific Computing Center, which is supported by the Office of Science of the U.S. Department of Energy under Contract No. DE-AC02-05CH11231.

APPENDIX: CORRELATION FUNCTIONS AND FOURIER TRANSFORMS

Starting from Eq. (5) defining the intermolecular potential, the S_2 matrix elements may be expressed in terms of the 2-D correlation functions defined as[11–13]

$$\begin{aligned} G_{L_1K_1K_1'L_2K_2K_2'}(t,t') = & \frac{1}{4\pi\hbar^2(2L_1+1)^2(2L_2+1)^2} \\ & \times \sum_L (-1)^{L_1+L_2+L} \times (2L+1) \\ & \times U(L_1L_2L; K_1K_2; R(t)) \\ & \times U(L_1L_2L; K_1'K_2'; R(t'))\, P_L[\Theta(t,t')], \end{aligned} \tag{A1}$$

where $\Theta(t,t')$ is the angle between $\vec{R}(t)$ and $\vec{R}(t')$. As explained in our previous works,[11,13] it is better to use their symmetric partners $\mathbb{G}_{L_1K_1K_1'L_2K_2K_2'}(\tau,\tau')$ obtained by changing the variables t and t′ to the variables $\tau \equiv t - t'$ and

$\tau' \equiv {}^1/_2(t + t')$,

$$\mathbb{G}_{L_1K_1K_1'L_2K_2K_2'}(\tau,\tau') = G_{L_1K_1K_1'L_2K_2K_2'}\left(\tau' + \frac{\tau}{2}, \tau' - \frac{\tau}{2}\right). \quad \text{(A2)}$$

The real parts of the diagonal elements of S_2 can be expressed in terms of symmetric 1-D Fourier transform, which are real and symmetric functions of ω, and defined by

$$\mathbb{F}_{L_1K_1K_1'L_2K_2K_2'}(\omega) = \frac{1}{\sqrt{2\pi}} \int_{-\infty}^{\infty} d\tau e^{i\omega\tau} \mathbb{G}_{L_1K_1K_1'L_2K_2K_2'}(\tau), \quad \text{(A3)}$$

where

$$\mathbb{G}_{L_1K_1K_1'L_2K_2K_2'}(\tau) = \int_{-\infty}^{\infty} d\tau' \mathbb{G}_{L_1K_1K_1'L_2K_2K_2'}(\tau,\tau'). \quad \text{(A4)}$$

For the off-diagonal elements of $S_{2,\text{middle}}$, it is necessary to introduce symmetric 2-D Fourier transforms defined by

$$\mathbb{F}_{L_1K_1K_1'L_2K_2K_2'}(\omega,\omega') = \frac{1}{2\pi} \int_{-\infty}^{\infty}\int_{-\infty}^{\infty} d\tau d\tau' e^{i\omega\tau} e^{i\omega'\tau'} \mathbb{G}_{L_1K_1K_1'L_2K_2K_2'}(\tau,\tau'). \quad \text{(A5)}$$

We note that for simplifying notations, the same symbols are used to represent the 2-D and 1-D correlation functions. Readers can distinguish them by the number of arguments. Because $\mathbb{G}_{L_1K_1K_1'L_2K_2K_2'}(\tau,\tau')$ are even functions of τ and τ′, their Fourier transforms are real and they are even functions of ω and ω′.

[1]J. M. Hartmann, C. Boulet, and D. Robert, *Collisional Effects on Molecular Spectra. Laboratory Experiments and Models, Consequences for Applications* (Elsevier, Amsterdam, 2008).
[2]J. M. Hartmann, H. Tran, and G. C. Toon, Atmos. Chem. Phys. **9**, 7303 (2009).
[3]A. Ben-Reuven, Phys. Rev. **145**, 34 (1966).
[4]R. Shafer and R. G. Gordon, J. Chem. Phys. **58**, 5422 (1973).
[5]F. Thibault, L. Gomez, S. V. Ivanov, O. G. Buzykin, and C. Boulet, J. Quant. Spectrosc. Radiat. Transfer **113**, 1887 (2012).
[6]G. Quéméner and N. Balakrishnan, J. Chem. Phys. **130**, 114303 (2009).
[7]S. V. Ivanov, C. Boulet, O. G. Buzykin, and F. Thibault, J. Chem. Phys. **141**, 184306 (2014).
[8]F. Niro, C. Boulet, and J. M. Hartmann, J. Quant. Spectrosc. Radiat. Transfer **88**, 483 (2004).
[9]J. Lamouroux, H. Tran, A. L. Laraia, R. R. Gamache, L. S. Rothman, I. E. Gordon, and J.-M. Hartmann, J. Quant. Spectrosc. Radiat. Transfer **111**, 2321 (2010).
[10]M. R. Cherkasov, J. Quant. Spectrosc. Radiat. Transfer **141**, 73 (2014).
[11]Q. Ma, C. Boulet, and R. H. Tipping, J. Chem. Phys. **139**, 034305 (2013).
[12]C. Boulet, Q. Ma, and F. Thibault, J. Chem. Phys. **140**, 084310 (2014).
[13]Q. Ma, C. Boulet, and R. H. Tipping, J. Chem. Phys. **140**, 104304 (2014).
[14]F. Niro, F. Hase, C. Camy-Peyret, S. Payan, and J. M. Hartmann, J. Quant. Spectrosc. Radiat. Transfer **90**, 43 (2005).
[15]F. Niro, T. Von Clarmann, K. Jucks, and J. M. Hartmann, J. Quant. Spectrosc. Radiat. Transfer **90**, 61 (2005).
[16]S. Green, J. Chem. Phys. **90**, 3603 (1989).
[17]R. P. Leavitt, J. Chem. Phys. **73**, 5432 (1980).
[18]R. R. Gamache, J. Lamouroux, A. L. Laraia, J. M. Hartmann, and C. Boulet, J. Quant. Spectrosc. Radiat. Transfer **113**, 976 (2012).
[19]N. N. Filippov and M. V. Tonkov, J. Chem. Phys. **108**, 3608 (1998).
[20]A. P. Kouzov, Phys. Rev. A **60**, 2931 (1999).
[21]Q. Ma, R. H. Tipping, G. Birnbaum, and C. Boulet, J. Quant. Spectrosc. Radiat. Transfer **59**, 259 (1998).
[22]C. Cousin, R. Le Doucen, C. Boulet, A. Henry, and D. Robert, J. Quant. Spectrosc. Radiat. Transfer **36**, 521 (1986).
[23]J. Boissoles, C. Boulet, and X. Bruet, J. Chem. Phys. **116**, 7537 (2002).
[24]E. W. Smith, J. Chem. Phys. **74**, 6658 (1981).
[25]C. G. Gray and K. E. Gubbins, *Theory of Molecular Fluids* (Clarendon, Oxford, 1984).
[26]H. Yasuda and T. Yamamoto, Prog. Theor. Phys. **45**, 1458 (1971).
[27]J. P. Bouanich, J. Quant. Spectrosc. Radiat. Transfer **47**, 243 (1992).
[28]M. Afzelius, P. Bengtsson, and J. Bonamy, J. Chem. Phys. **120**, 8616 (2004).
[29]J. Boissoles, C. Boulet, D. Robert, and S. Green, J. Chem. Phys. **87**, 3436 (1987).
[30]N. N. Filippov and M. V. Tonkov, J. Quant. Spectrosc. Radiat. Transfer **50**, 111 (1993).
[31]J. Boissoles, C. Boulet, D. Robert, and S. Green, J. Chem. Phys. **90**, 5392 (1989).
[32]L. Ozanne, Nguyen-Van-Thanh, C. Brodbeck, J. P. Bouanich, J. M. Hartmann, and C. Boulet, J. Chem. Phys. **102**, 7306 (1995).
[33]W. D. Gillespie, C. J. Meinrenken, W. R. Lempert, and R. B. Miles, J. Chem. Phys. **107**, 5995 (1997).
[34]A. Predoi-Cross, W. Liu, C. Holladay, A. V. Unni, I. Scoffield, A. R. W. McKellar, and D. R. Hurtmans, J. Mol. Spectrosc. **246**, 98 (2007).
[35]M. Margottin-Maclou, P. Dahoo, A. Henry, A. Valentin, and L. Henry, J. Mol. Spectrosc. **131**, 21 (1988).
[36]N. N. Filippov, R. E. Asfin, T. N. Sinyakova, I. M. Grogoriev, T. M. Petrova, A. M. Solodov, A. A. Solodov, and J. V. Buldyreva, Phys. Chem. Chem. Phys. **15**, 13826 (2013).
[37]See supplementary material at http://dx.doi.org/10.1063/1.4931587 for all the calculated relaxation matrices in the present study.